**Supplementary Note 1: Beam measurement and avalanche breakdown volume**

The λ=1024 nm pump pulses were focused to Gaussian waists ($1/e^2$ intensity radius) of $w_0$=8 μm ($I < 100$ TW/cm$^2$, Rayleigh range $z_0$~0.2 mm) or $w_0$= 26 μm ($I < 10$ TW/cm$^2$, $z_0$~2 mm) for $\theta = 90°$, while for $\theta = 0°$, they were focused to $w_0$= 30 μm. The λ=3.9μm pump pulses were focused to $w_0$=39 μm ($z_0$~1.2 mm, up to 10 TW/cm$^2$) for $\theta = 90°$. Near-IR and mid-IR peak pump intensities were determined by measuring focal spots directly on a CCD camera or an InSb array, respectively. Pulse duration measurements made with using an autocorrelator (for λ=1024 nm) or with scanning second-harmonic generation frequency resolved optical gating, or SHG-FROG (for λ=3.9 μm). Uncertainty in pulse duration ($\pm\sim 5$ %) and focused beam spot size ($\pm\sim$4% due to finite pixel size) gives absolute uncertainty of $\sim \pm 10\%$ in measured intensity values. Breakdown occurs if electron growth from heating and subsequent ionization exceeds losses due to recombination, attachment, and diffusion out of the laser focal volume, leading to a characteristic intensity threshold [1-4]. For short pulses, this breakdown criterion is increased in order to drive avalanche to some detectable threshold before the end of the pulse, which in this case was detection of a visible breakdown site in images of the interaction region. Images were collected at 2× magnification on the CMOS camera, and the number of breakdowns was determined by counting the number of sites with peak signals above 20 pixel counts after median filtering. In order to determine the breakdown threshold for different gases and pressures, probe pulse peak power was reduced until the pump-seeded breakdowns at the center of the probe volume (peak probe intensity) were barely visible (~20 pixel counts). This gave a breakdown threshold $I_{th}\sim 1$ TW/cm$^2$ in nitrogen and air, and 0.6 TW/cm$^2$ in argon, with a $1/p$ pressure dependence for all gases studied, in line with past observations [1]. When counts were converted to yield during data collection (peak intensity typically ~$1.5I_{th}$), integration was performed over the volume of the probe beam where $I > I_{th}$, as determined by direct measurements of the probe beam waist and the beam longitudinal profile.

**Supplementary Note 2: Effect of filter on contaminant breakdowns and scaling of self-seeded (probe produced) breakdowns**

Contaminant breakdowns were observed in all gases at a similar level, which included lab compressed air (filtered for oil/moisture and particulates) and high purity argon and nitrogen (Praxair, Ultrahigh Purity 5.0, <3 parts-per-million (ppm) water, <0.5 ppm total hydrocarbon content). When air passed through the particulate filter was replaced with bottled ultra-high purity air (Praxair, Ultra Zero, <2 ppm water, <0.1 ppm total hydrocarbon content) passed through an activated charcoal Supelcarb hydrocarbon filter (capable of filtering primary hydrocarbons to ~the part-per-billion level) for identical pump conditions ($\lambda = 3.9\,\mu m, \theta = 90°$), the number of breakdown counts decreased by ~4×, as shown in Fig. S1.

Since counts could not be observed below ~5 TW/cm$^2$ in this configuration and pumping in the $\theta = 0°$ geometry with the $\lambda = 3.9\,\mu m$ pump was experimentally difficult, low yield ionization was tested using breakdown counts initiated by "self-seeded" electrons, or seed electrons produced by the leading edge of the 50 ps, ~1.5 TW/cm$^2$ probe pulse which were subsequently amplified and detected as breakdown counts generated by the remainder of the pulse. Figure S2 shows both raw counts for 1.5-1.8 TW/cm$^2$, and corrections for the increase in size of the breakdown volume with increasing intensity and the increase in the time during which

electrons can be liberated and amplified. Namely, if single electron-seeded breakdowns at a local intensity of 1.8 TW/cm$^2$ occur

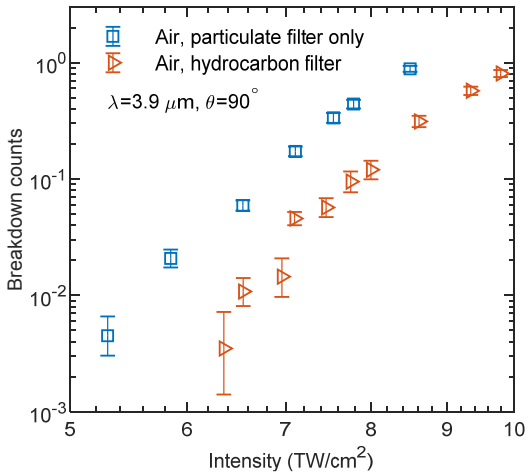


**Fig. S1 | Effect of hydrocarbon filter on yield measurements in air.** Breakdown counts observed with the λ=3.9 μm pump for two sources of air: (i) air passed through only the particulate filter or (ii) ultra-high purity compressed air from a bottle fitted with an additional part-per-billion hydrocarbon trap.

in 27 ps while breakdowns at 1.5 TW/cm$^2$ occur in ~33 ps, the second pulse has 6 ps longer in which to ionize contaminants through MPI and still drive a detectable breakdown. While the correction is simplistic (applying changes in volume and timing as a constant multiplicative factor
and ignoring spatial variations in yield and timing), it gives a rough estimate of the scaling in this regime. In particular, it shows that counts are still driven by MPI/tunneling, with a best fit of the corrected counts giving $Y_{3.9\mu m} \propto I^{19\pm8}$. To incorporate this data into Fig. 3 of the main text, the data was normalized to the data taken with the 85 fs pump pulse by accounting for the ratio in volumes between the self-seeding case and the $\theta = 90°$ geometry (~300) and the change in pulse length and temporal shape (~1000×). This normalization gives a yield in reasonable agreement with the theoretical curve, and consistent with a contaminant with ionization potential ~6 eV. The strong intensity scaling of probe self-seeded breakdowns also explains the variation in background breakdown counts, since small changes in probe intensity (~10-15% uncertainty for different configurations, or intraday and day-to-day drifts) can lead to large changes in background rates. A slightly lower probe peak intensity for the $\theta = 0°$ experiment of Fig. 2 led to the ~10× reduction in probe self-seeded background counts compared to the $\theta = 90°$ geometry, despite the larger pump-probe overlap volume.

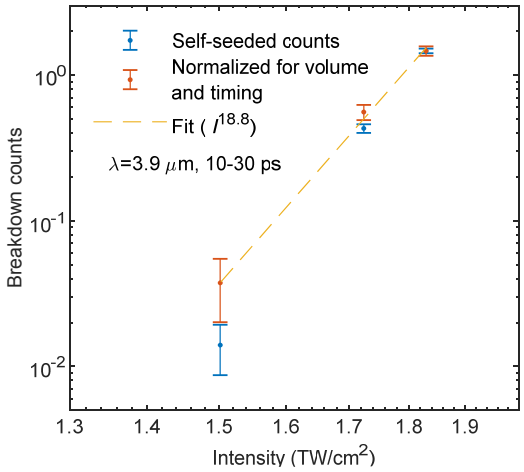


**Fig. S2 | Scan of self-seeded counts.** Number of breakdowns observed for varying probe (only) pulse intensities, with seed electrons liberated via MPI by the leading edge of the pulse. Also shown is a correction for changes in breakdown volume and effective seed timing as probe intensity is increased. A best fit of the points gives scaling $Y_{3.9\mu m} \propto I^{19\pm8}$, with the large uncertainty set by the limited range of results.

## Supplementary Note 3: Avalanche breakdown timing, simulations, and density estimation from time advance measurements

For a single electron seed, the time required to reach a specific breakdown condition is determined entirely by the local intensity, which in turn determines electron heating, temperature, and growth rate. However, if only a few seed electrons are randomly placed within the breakdown region, the time required to reach breakdown will show statistical variation due to spatial variations in intensity [5]. As the density of seeds is increased, there is a high probability of an electron being found in the region of highest intensity, leading to a deterministic breakdown time. As mentioned in the main text, once two seed electrons are closer than the diffusion length, the time required to reach saturation will decrease further, since the number of doublings in electron number (generations) will be reduced [2,6].

Breakdown timing was measured by observing the spectrum of pump light backscattered from the interaction region. Since the pump pulse is positively chirped to a length of 50 ps FWHM (70 ps full width) from its bandwidth-limited duration of ~80 fs, each spectral component corresponds to particular time slice in a 70 ps window. Energy backscattered from the plasma is detected with a single-shot mid-IR spectrometer, with a cryogenically cooled InSb detector, with a minimum electron density of ~$10^{17}$-$10^{18}$ cm$^{-3}$ required for detection of the backscatter signal, based on the analysis in [7] and its supplementary material. The longest wavelength above the detector noise threshold was recorded for each shot, and then breakdown timing was determined by the time-frequency mapping determined through a cross correlation measurement.

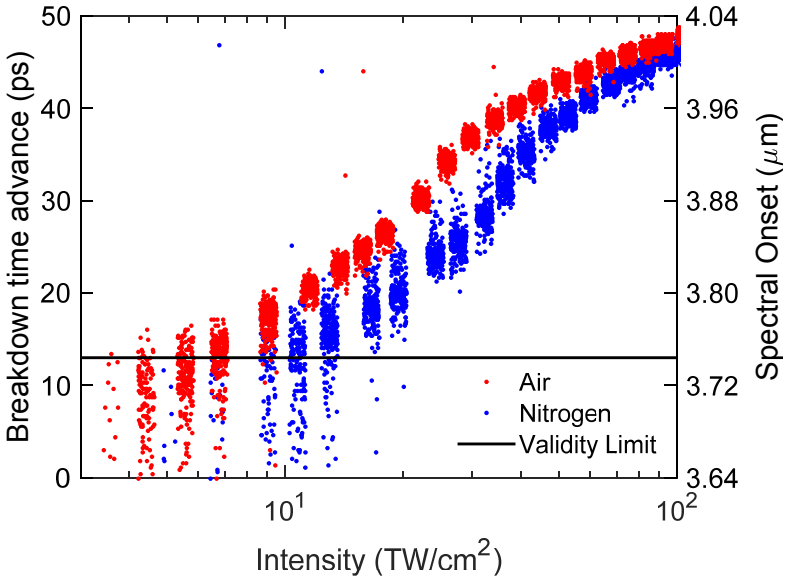


**Fig. S3 | Single shot breakdown timing.** Each point corresponds to a single probe pulse backscattered spectrum measurement, with the right vertical scale showing the longest wavelength detected, and the associated breakdown time advance shown on the left vertical scale. For low pump intensities, liberated electrons, when they are generated at all, are randomly positioned in the probe breakdown volume, leading to a spread of breakdown times. As pump intensity is increased, multiple seed electrons are generated and more are likely to be found at the peak probe intensity, which visually corresponds to ~13 ps time advance. As more breakdowns occur, they begin to overlap, leading to a deterministic decrease in breakdown timing (>13 ps advance), with the spread in points in that part of the plot determined by fluctuations in probe intensity.

For the present experiment, the width of the breakdown volume (region above threshold) for driving avalanche and backscattering was ~40μm, while the diffusion-limited diameter of single-electron-seeded breakdown plasmas was ~10μm during their initial growth phase. Thus, even when a single breakdown occurs on every shot, timing measured by backscatter will be variable because a single pump-generated seed electron could find itself in a range of intensities above the breakdown threshold. This is seen in Figure S3, where the points at ~<6 TW/cm$^2$ show a timing variation even though there is a ~1 breakdown/shot at that intensity. Once ~4-8 seed electrons are distributed in the breakdown region, there is a higher probability that one seed electron is located at the region of peak probe intensity, leading to more deterministic timing. Above ~8-10 seed electrons in the breakdown region, there is a high probability of 2 electrons being located at the region of peak intensity and within ~10μm of each other, such that number of generations needed to reach the detection threshold is reduced by one. This leads to our estimate that time advance is directly correlated with density for yields above $7 \times 10^{-11}$cm$^{-3}$, namely 10 times the yield corresponding to ~1 breakdown per shot calculated in Fig. 2 of the main text. On the plot of time advance, this density is then used to match the time advance where statistical breakdown ends, as shown in Fig. S3. Yields at 100 TW/cm$^2$ were matched exactly with the standard theoretical rate [8], since measurements of $O_2$ and $N_2$ yield in a thin gas jet with a 42 fs, 800 nm pulse at this intensity [9] showed excellent agreement with the theoretical rate for this same intensity range. Interpolating between the two gives an electron density growth rate of $\nu = 0.55\ \mathrm{ps}^{-1}$ during the probe pulse, which was used to calculate the intermediate densities. We note that our chirped probe pulse temporal profile is not exactly square, with a spectral measurement of the OPCPA's mid-IR beam and its near-IR conjugate suggesting more

power at the beginning of the pulse, so that ponderomotive heating ($\propto I\lambda^2$) will be stronger at the beginning of the chirped pulse than at the end. Accounting for this would tend to suppress the inferred density slightly throughout the range, bringing it into closer agreement with the theoretical rate.

It is worth noting that the backscattering method does not rely on simulations, which in turn are dependent on accurate rates for elastic and inelastic collisions, attachment, diffusion, and transport. Nevertheless, a comparison with simulations can give confidence in the general approach. Using a constant intensity of 1.3 TW/cm$^2$ (the peak probe intensity used for high yield measurements) in a self-consistent set of 0-D equations that track the temperature of avalanching electrons through electron-neutral collisions (heating), and attachment, excitation, dissociative and ionization losses, [2,6] predicts a growth rate of $\nu = 0.35\ \mathrm{ps}^{-1}$ after ~2 ps of initial heating needed to reach a steady state plasma temperature of 10 eV. This matches reasonably well with the growth rate assumed by observing the 35 ps change in initial density of $2 \times 10^8$ from Fig. 4 of the main text, which gives a growth rate of $\nu = 0.55\ \mathrm{ps}^{-1}$. We note that the simulations are sensitive to uncertainty in loss rates and collision rates, as well as any departure from the assumption of a thermal electron distribution, so disagreement is not unexpected.

## References


1. C. G. Morgan, Rep. Prog. Phys. **38**, 621 (1975).
2. J. Isaacs *et al*., Phys. Plasmas **23**, 033507 (2016).
3. A. W. Ali. NRL Memorandum Report 5187 (1983).
4. A. W. Ali. NRL Memorandum Report 5400 (1984).
5. R. M. Schwartz *et al*., Sci. Adv. **5**, eaav6804 (2019).
6. J. Isaacs *et al*., Proc. SPIE, **11010**, 11010E (2019).
7. D. Woodbury *et al*., Optica **6**, 811 (2019).
8. S. V. Popruzhenko *et al*., Phys. Rev. Lett. **101**, 193003 (2008).
9. J.K. Wahlstrand *et al*., Phys. Rev. Lett. **120**, 183901 (2018).